

Baryon states with hidden charm in the extended local hidden gauge approach

T. Uchino,^{1,*} Wei-Hong Liang,² and E. Oset¹

¹*Departamento de Física Teórica and IFIC, Centro Mixto Universidad de Valencia-CSIC, Institutos de Investigación de Paterna, Apartado 22085, 46071 Valencia, Spain*

²*Department of Physics, Guangxi Normal University, Guilin, 541004, People's Republic of China*

(Dated: August 14, 2021)

Abstract

The s -wave interaction of $\bar{D}\Lambda_c$, $\bar{D}\Sigma_c$, $\bar{D}^*\Lambda_c$, $\bar{D}^*\Sigma_c$ and $\bar{D}\Sigma_c^*$, $\bar{D}^*\Sigma_c^*$, is studied within a unitary coupled channels scheme with the extended local hidden gauge approach. In addition to the Weinberg-Tomozawa term, several additional diagrams via the pion-exchange are also taken into account as box potentials. Furthermore, in order to implement the full coupled channels calculation, some of the box potentials which mix the vector-baryon and pseudoscalar-baryon sectors are extended to construct the effective transition potentials. As a result, we have observed six possible states in several angular momenta. Four of them correspond to two pairs of admixture states, two of $\bar{D}\Sigma_c - \bar{D}^*\Sigma_c$ with $J = 1/2$, and two of $\bar{D}\Sigma_c^* - \bar{D}^*\Sigma_c^*$ with $J = 3/2$. Moreover, we find a $\bar{D}^*\Sigma_c$ resonance which couples to the $\bar{D}\Lambda_c$ channel and one spin degenerated bound state of $\bar{D}^*\Sigma_c^*$ with $J = 1/2, 5/2$.

arXiv:1504.05726v1 [hep-ph] 22 Apr 2015

* uchino@ific.uv.es

I. INTRODUCTION

In this work, possible nucleon resonances with negative parity are studied, with the energy around $4200 \sim 4400$ MeV, which are found as molecular states of one anti-charmed meson, \bar{D} or \bar{D}^* , and a charmed baryon. Here the local hidden gauge approach with an extension to $SU(4)$ is utilized, as done in Refs. [1–4] to deal with the hadronic interaction involving heavy quarks. Within the framework of the local hidden gauge approach, the meson-baryon scattering proceeds via the vector-exchange [5–7] (see also Ref. [8] for practical rules) and the interaction kernel projected over s -wave results in the form of the Weinberg-Tomozawa interaction [3, 4, 9–13]. The heavy quark spin symmetry (HQSS) is known to play an important role in the heavy quark sector [14–17] and has been utilized to investigate the hadron spectroscopy in the high energy region [1, 18–24]. Yet, it was also found in Ref. [1] that the extension of the local hidden gauge approach automatically fulfils the rules of HQSS.

Compared to the light quark sector, more importance should be placed on the vector-pseudoscalar admixture because of the small mass difference between them, namely $m_{D^*} - m_D \sim 140$ MeV in the charm sector while $m_{K^*} - m_K \sim 500$ MeV. In the meson-baryon scattering, the mixing of vector-baryon (VB) and pseudoscalar-baryon (PB) sectors proceeds via the pion-exchange induced by the $\bar{D}\bar{D}^*\pi$ vertex, which is one of the ingredients of the local hidden gauge approach [5–7, 25–27]. When dealing with pion exchange, the on-shell factorization of the potential, which is done for vector exchange in the chiral unitary approach, is not possible because of the momentum dependence of the pion exchange. This is why the dynamics of pion exchange is included by means of a box diagrams, mediated by pion exchange, with the excitation of the corresponding meson-baryon intermediate states [25, 26]. The pion exchange between pseudoscalar and vector mesons is accompanied by the contact Kroll-Ruderman term [25, 28] which breaks the spin degeneracy of the vector-baryon states in the absence of this interaction [27].

In addition to the vector-pseudoscalar mixing term, another pion exchange contribution which stems from the anomalous $\bar{D}^*\bar{D}^*\pi$ vertex is also taken into account [27]. This interaction does not interfere with the s -wave driving force of the Weinberg-Tomozawa term, and hence it also goes via the pion-exchange in the box diagram. This box diagram involving the anomalous coupling contributes only to the VB sectors as an attractive potential. When a VB channel develops a bound state, the corresponding PB channel also generates a bound state and the generated state of the VB sector should be heavier than that of the PB sector due to the mass difference of \bar{D}^* and \bar{D} . However, thanks to the extra attraction coming from the anomalous term, the VB sector binds more and hence the mixing effect of the VB and PB sectors now becomes more noteworthy.

In this work, we go further with our approach to the VB and PB mixing by implementing the full coupled channels calculation. Indeed, the VB sector can couple to the PB sector via the pion exchange interaction, however this exchange carries momentum transfer and thus in the multiple scattering it is not straightforward to factorize the relevant terms concerning this VB - PB mixing. Then we implement the full coupled channels calculation by constructing effective $VB \leftrightarrow PB$ transition potentials from the corresponding box diagrams as done in Ref. [27]

Eventually, six nucleon resonances are generated within the framework of the full coupled channels calculation based on the extended local hidden gauge approach with the anomalous term with several quantum numbers. In addition to the masses and widths of the states, their building blocks or main components are evaluated by the wave function at the origin,

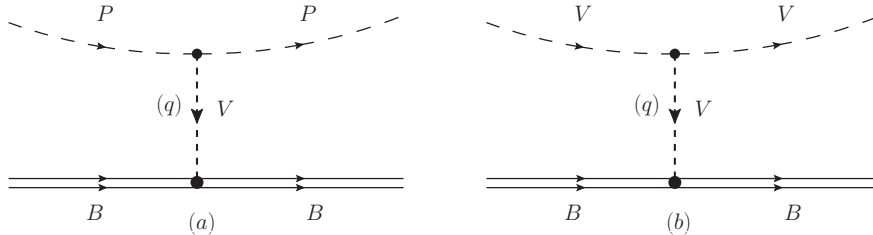


FIG. 1. Diagrammatic representation of the pseudoscalar-baryon interaction (a) and vector-baryon interaction (b).

as discussed in Ref. [29]. One of the remarkable observations is the appearance of pairs of orthogonal states mixing the same PB and VB states. In the previous work on open charm baryons [27], in addition to $\Lambda_c(2592)$ which has experimentally been observed, its orthogonal state with an energy 2767 MeV was also generated. Similarly, in this work two pairs of orthogonal states are also deduced. Moreover, as HQSS is incorporated implicitly within the driving force, the results resemble pairs of heavy quark spin symmetry partners. The meson-baryon hidden charm sector was studied along the same line in Refs. [3, 4] but without including pion exchange and hence not mixing the PB and VB states. We shall comment on the analogies and the differences found here with respect to that work. We shall also comment on results of other works that use $SU(8)$ spin-flavour symmetry [23] or quark model [44].

II. FORMALISM

A. The interaction via the vector-exchange

We study the isospin $I = 1/2$ hidden charm states, the N^* resonances with the energy around 4200 \sim 4400 MeV, following the local hidden gauge approach [5–7]. In Refs. [1, 4], the same states have been investigated within the local hidden gauge approach extended to $SU(4)$. The validity of the use of $SU(4)$ in this kind of studies has been widely discussed in Refs. [13, 27, 30]. Although $SU(4)$ is broken at the end as a consequence of the multiple scattering and the different masses of the particles within a same multiplet, the elementary vertices which we use here are rather $SU(4)$ symmetric and its use within the present context is acceptable.

We will use the coupled channels formed with anti-charmed mesons \bar{D} and \bar{D}^* and charmed baryons Λ_c , Σ_c , Σ_c^* , Λ_c , namely $\bar{D}\Lambda_c$, $\bar{D}\Sigma_c$, $\bar{D}^*\Lambda_c$, $\bar{D}^*\Sigma_c$, $\bar{D}\Sigma_c^*$, $\bar{D}^*\Sigma_c^*$. In Ref. [4], the lighter states such as $\eta_c N$, πN , ηN , $\eta' N$, $K\Sigma$, $K\Lambda$ for the PB sector, were included as a correction (a similar procedure was also considered for the VB sector), however, these states were found not to modify the energies and simply gave around 30 MeV width to the generated states. In the present work, we do not consider these states but will keep in mind that the states generated that can couple to these states will have a width of that order of magnitude at least.

According to the local hidden gauge approach, the meson-baryon interaction proceeds via the exchange of vector mesons as depicted in Fig. 1. Neglecting the three momenta carried by the exchanged vector, as is automatically done in these studies, we obtain the s -wave

potential of the PB scattering from channel i to channel j [31]

$$V_{ij} = -C_{ij} \frac{1}{4f^2} (2\sqrt{s} - M_{B_i} - M_{B_j}) \sqrt{\frac{M_{B_i} + E_i}{2M_{B_i}}} \sqrt{\frac{M_{B_j} + E_j}{2M_{B_j}}}, \quad (1)$$

with $f = f_\pi = 93$ MeV being the pion decay constant, M_{B_i} , E_i (M_{B_j} , E_j) the mass, energy of baryon of i (j) channel. In the case of the VB scattering, the interaction kernels and the following scattering amplitudes have an extra factor $\vec{\epsilon} \cdot \vec{\epsilon}'$, the scalar product of the polarization vectors of the incoming and outgoing vector mesons. The coefficients of Eq. (1) are given in Tables A1, A2, A3 and A4 in the Appendix.

As we shall see in Sec. II C, in addition to the vector-exchange interaction of Eq. (1), the pion exchange interaction is also taken into account which stems from the local hidden gauge scheme too. This contribution is responsible for mixing the PB and VB sectors and breaking the spin degeneracy as studied in Refs. [25–27, 32–34].

B. The construction of the scattering matrix

With the interaction kernel V_{ij} of Eq. (1), we evaluate the PB or VB two body scattering amplitudes. By solving the Bethe-Salpeter equation in coupled channels, we obtain the scattering amplitude T given in a matrix form

$$T = [1 - V G]^{-1} V, \quad (2)$$

with G being the diagonal loop function which stands for the propagation of the intermediate meson-baryon states. As pointed out in Refs. [2, 13], the use of the G function with the dimensional regularization scheme can generate unphysical states below the threshold. Hence, in this work, we utilize the G function regularized with the cut off scheme

$$G(s) = \int_0^{q_{\max}} \frac{d^3\vec{q}}{(2\pi)^3} \frac{\omega_P + \omega_B}{2\omega_P\omega_B} \frac{2M_B}{P^0 - (\omega_P + \omega_B)^2 + i\epsilon}, \quad (3)$$

where P^0 is the CM energy, $s = (P^0)^2$, $\omega_P = \sqrt{\vec{q}^2 + m_P^2}$, $\omega_B = \sqrt{\vec{q}^2 + M_B^2}$, and q_{\max} is the cut-off of the three-momentum.

Here, let us refer to a problem which occurs in the cut off method too. The G function with the cut off method also has deficiencies if the cut off is not reasonably larger than the on shell momentum of the intermediate state. This can only affect the $\bar{D}\Lambda_c$ channel in our approach. But the interaction of the $\bar{D}\Lambda_c$ channel is repulsive and does not lead to bound states in this channel. This channel has only a weak and indirect effect in our results which will be discussed below.

C. Breaking the spin degeneracy in vector-baryon sectors

In this subsection we break the spin degeneracy in the VB sector, namely that of the \bar{D}^*B states. Following the approach of Refs. [25, 32, 33, 35], we mix states of \bar{D}^*B_a and $\bar{D}B_b$ states in both spin channels as a box diagram such as $\bar{D}^*B_a \rightarrow \bar{D}B_b \rightarrow \bar{D}^*B_a$ and vice versa, in a first step. Later on we will revert to full coupled channels. The procedure to

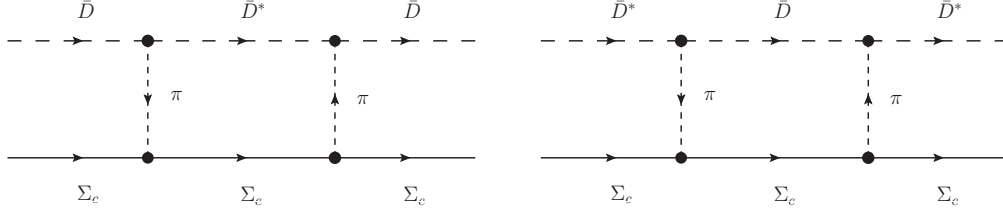


FIG. 2. Diagrammatic representation of the $\bar{D}^*\Sigma_c$ in the intermediate state (left) and the $\bar{D}\Sigma_c$ in the intermediate state (right).

evaluate these diagrams follows closely what has been done before in the open charm case [27], but in the baryon sector we have more baryons to take into account, while in Ref. [27] only nucleons were involved.

We consider the following $PB \leftrightarrow VB$ mixing processes

$$\begin{aligned}
\bar{D}\Sigma_c &\rightarrow \bar{D}^*\Sigma_c \rightarrow \bar{D}\Sigma_c, & \bar{D}^*\Sigma_c &\rightarrow \bar{D}\Sigma_c \rightarrow \bar{D}^*\Sigma_c, \\
\bar{D}\Sigma_c &\rightarrow \bar{D}^*\Lambda_c \rightarrow \bar{D}\Sigma_c, & \bar{D}^*\Lambda_c &\rightarrow \bar{D}\Sigma_c \rightarrow \bar{D}^*\Lambda_c, \\
\bar{D}\Sigma_c^* &\rightarrow \bar{D}^*\Sigma_c^* \rightarrow \bar{D}\Sigma_c^*, & \bar{D}^*\Sigma_c^* &\rightarrow \bar{D}\Sigma_c^* \rightarrow \bar{D}^*\Sigma_c^*, \\
\bar{D}^*\Sigma_c &\rightarrow \bar{D}\Lambda_c \rightarrow \bar{D}^*\Sigma_c.
\end{aligned}$$

In the mixing we omit the transitions involving the $\pi\Sigma_c\Sigma_c^*$ vertex. The reason is that the SU(4) Clebsch-Gordan coefficient for this vertex is $1/\sqrt{12}$ compared with $1/\sqrt{2}$ for the $\pi N\Delta$. Given the moderate role played by $\pi N\Delta$ transition found in Ref. [26], this approximation is a fair simplifying option. The Clebsch-Gordan coefficient for $\pi\Lambda_c\Sigma_c^*$ is $1/\sqrt{4}$, not so small compared to that of $\pi N\Delta$, but given the fact that the $\bar{D}\Lambda_c$ and $\bar{D}^*\Lambda_c$ channels do not generate bound states by themselves and play only a minor, indirect role in the study, we also neglect terms involving this vertex from the beginning. In addition, note that the $\pi\Lambda_c\Lambda_c$ vertex is zero due to isospin conservation.

In Fig. 2, a pair of the $\bar{D}\Sigma_c$ and $\bar{D}^*\Sigma_c$ box diagrams, is shown. As discussed in Sec. II B, we include the $\bar{D}\Lambda_c$ channel only as an intermediate state in the $\bar{D}^*\Sigma_c$ box diagram. Then the channels with Σ_c^* are completely separated from the others with Σ_c or Λ_c .

First we show the construction of the box potentials with the baryons, Λ_c or Σ_c . We detail the calculation for $\bar{D}\Sigma_c \rightarrow \bar{D}^*\Sigma_c \rightarrow \bar{D}\Sigma_c$ and use the result as reference to obtain the result in the other cases. By using the $\bar{D}(\bar{D}^*)$ isospin doublet, (\bar{D}^0, D^-) and $\Sigma_c(\Sigma_c^*)$ triplet, $(-\Sigma_c^{++}, \Sigma_c^+, \Sigma_c^0)$, we write down the relevant hidden charm states with $I = 1/2$ in the charge basis

$$|\bar{D}\Sigma_c, I = 1/2, I_3 = +1/2\rangle = \sqrt{\frac{2}{3}}|D^-\Sigma_c^{++}\rangle + \sqrt{\frac{1}{3}}|\bar{D}^0\Sigma_c^+\rangle, \quad (4)$$

$$|\bar{D}\Lambda_c, I = 1/2, I_3 = +1/2\rangle = |\bar{D}^0\Lambda_c^+\rangle, \quad (5)$$

and analogously for their excited states such as $\bar{D}^*\Sigma_c$, $\bar{D}\Sigma_c^*$, $\bar{D}^*\Sigma_c^*$ and $\bar{D}^*\Lambda_c$. In order to evaluate the $\bar{D}\Sigma_c \rightarrow \bar{D}^*\Sigma_c$ transition in $I = 1/2$, we must consider the diagrams depicted in Fig. 3, and technically, as also done in Refs. [26, 27], we evaluate the transitions using only SU(3) symmetry by working in the (u, d, s) sector and using the correspondence of the (K^+, K^0) and $(\bar{K}^0, -K^-)$ isospin doublets with the (\bar{D}^0, D^-) and $(D^+, -D^0)$ ones,

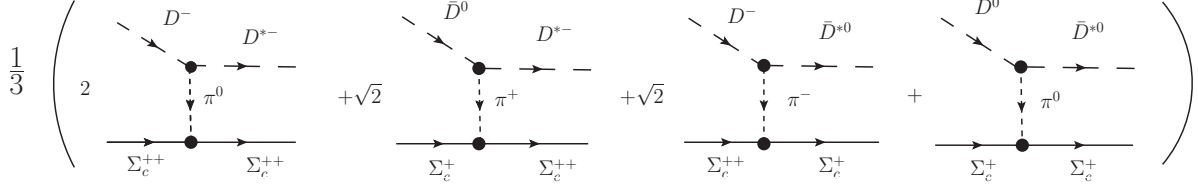


FIG. 3. Diagrammatic representation of the transition $\bar{D}\Sigma_c \rightarrow \bar{D}^*\Sigma_c$ in $I = 1/2$.

respectively. We need the VPP Lagrangian

$$\mathcal{L}_{VPP} = -ig \langle [P, \partial_\mu P] V^\mu \rangle, \quad (6)$$

where P , V^μ are the ordinary pseudoscalar octet and vector nonet SU(3) matrices of the corresponding fields

$$P = \begin{pmatrix} \frac{\pi^0}{\sqrt{2}} + \frac{\eta_8}{\sqrt{6}} & \pi^+ & K^+ \\ \pi^- & -\frac{\pi^0}{\sqrt{2}} + \frac{\eta_8}{\sqrt{6}} & K^0 \\ K^- & \bar{K}^0 & -\frac{2\eta_8}{\sqrt{6}} \end{pmatrix}, \quad (7)$$

$$V_\mu = \begin{pmatrix} \frac{\rho^0}{\sqrt{2}} + \frac{\omega}{\sqrt{2}} & \rho^+ & K^{*+} \\ \rho^- & -\frac{\rho^0}{\sqrt{2}} + \frac{\omega}{\sqrt{2}} & K^{*0} \\ K^{*-} & \bar{K}^{*0} & \phi \end{pmatrix}_\mu. \quad (8)$$

and $g = m_V/2f_\pi$ with $m_V \approx 780$ MeV.

From the Lagrangian of Eq. (6) with Eqs. (7) and (8), the $K^* \rightarrow K\pi$ decay amplitude that corresponds to the $\bar{D}^* \rightarrow \bar{D}\pi$ process is obtained. Yet, in order to get the coupling in the charm sector, it is required to implement an extra factor to account for the different meson field normalizations ($1/\sqrt{2\omega_i}$) and then fulfil the HQSS rules, as pointed out in the previous study of the beauty sector [26]. In this case, for instance, the two transition amplitudes, $D^{*-} \rightarrow \bar{D}^0\pi^-$ and $K^{*0} \rightarrow K^+\pi^-$, are related as follows

$$\frac{t_{\bar{D}^* \rightarrow \bar{D}\pi}}{t_{K^* \rightarrow K\pi}} \equiv \frac{\sqrt{m_{D^*}m_D}}{\sqrt{m_{K^*}m_K}} \simeq \frac{m_{D^*}}{m_{K^*}}. \quad (9)$$

The analogy of the strange and charm sectors used before for the $\pi\bar{D}^*\bar{D}$ vertex is also used for the $\pi B\bar{B}$ vertex, using the correspondence of the isospin multiplets ($-\Sigma^+$, Σ^0 , Σ_c^-) and ($-\Sigma_c^{++}$, Σ_c^+ , Σ_c^0). Then we use the standard Yukawa coupling of pions to baryons in SU(3) [36, 37], and we obtain the amplitude for the $\bar{D}\Sigma_c \rightarrow \bar{D}^*\Sigma_c$ transition

$$\begin{aligned} -it_{\bar{D}\Sigma_c \rightarrow \bar{D}^*\Sigma_c}^P &= -\sqrt{2}g \frac{m_{D^*}}{m_{K^*}} (q + P_{\text{in}})_\mu \epsilon^\mu \frac{1}{q^2 - m_\pi^2} \frac{2F}{2f_\pi} \vec{\sigma} \cdot \vec{q} \\ &= 2\sqrt{2}g \frac{m_{D^*}}{m_{K^*}} \vec{q} \cdot \vec{\epsilon} \frac{1}{q^2 - m_\pi^2} \frac{2F}{2f_\pi} \vec{\sigma} \cdot \vec{q}, \end{aligned} \quad (10)$$

taking $D = 0.75$ and $F = 0.51$ [38] for the two couplings of the Yukawa vertex, where P_{in} , P_{out} are the incoming, outgoing meson momentum and q is the momentum transfer, and several relations, $P_{\text{in}} = q + P_{\text{out}}$ and $P_{\text{out}} \cdot \epsilon = 0$ plus $\epsilon^0 \approx 0$, are used. Note that

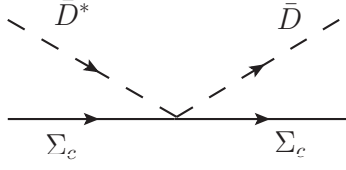


FIG. 4. Diagram of the Kroll Ruderman term.

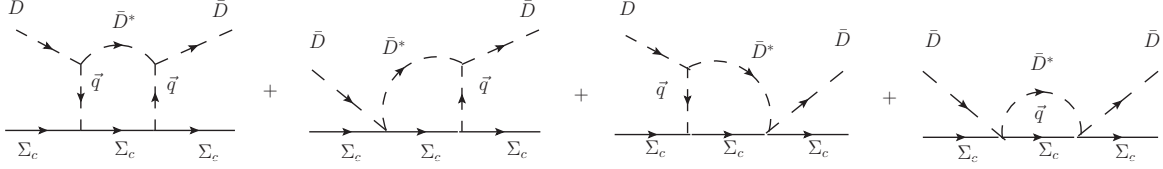


FIG. 5. The $\bar{D}\Sigma_c \rightarrow \bar{D}^*\Sigma_c \rightarrow \bar{D}\Sigma_c$ box diagrams.

we work close to the threshold of the vector-baryon channel, which justifies taking $\epsilon^0 = 0$. In addition to the pion exchange of Fig. 3, we should also consider the Kroll-Ruderman contact term from the gauge invariance constraint, as depicted in Fig. 4. By replacing $\epsilon_\mu(q + P_{\text{in}})^\mu \frac{1}{q^2 - m_\pi^2} \vec{\sigma} \cdot \vec{q}$ of Eq. (10) by $-\vec{\sigma} \cdot \vec{\epsilon}$, as discussed in Refs. [25, 28], we have the contact term

$$-it_{D\Sigma_c \rightarrow \bar{D}^*\Sigma_c}^C = \sqrt{2}g \frac{m_{D^*}}{m_{K^*}} \frac{2F}{2f_\pi} \vec{\sigma} \cdot \vec{\epsilon}. \quad (11)$$

With the two $\bar{D}\Sigma_c \rightarrow \bar{D}^*\Sigma_c$ transition amplitudes of Eqs. (10) and (11), we construct the potential for the $\bar{D}\Sigma_c \rightarrow \bar{D}^*\Sigma_c \rightarrow \bar{D}\Sigma_c$ box diagrams as shown in Fig. 5, and we obtain

$$\delta V = \delta V^{PP} + 2\delta V^{PC} + \delta V^{CC}, \quad (12)$$

where δV^{PP} stands for the first diagram of Fig. 5, $2\delta V^{PC}$ for the two middle diagrams and δV^{CC} for the last one. As shown in Refs. [25–27], we have the box potential of the $\bar{D}\Sigma_c \rightarrow \bar{D}^*\Sigma_c \rightarrow \bar{D}\Sigma_c$ process

$$\begin{aligned} -i\delta V^{PP} &= \int \frac{d^4q}{(2\pi)^4} \left(\frac{m_{D^*}}{m_{K^*}} \right)^2 g \left(2\sqrt{2}\vec{\epsilon} \cdot \vec{q} \frac{1}{q^{02} - \vec{q}^2 - m_\pi^2} \frac{2F}{2f_\pi} \vec{\sigma} \cdot \vec{q} \right) \\ &\quad \times (-g) \left(2\sqrt{2}\vec{\epsilon} \cdot \vec{q} \frac{1}{q^{02} - \vec{q}^2 - m_\pi^2} \frac{2F}{2f_\pi} \vec{\sigma} \cdot \vec{q} \right) \\ &\quad \times i \frac{1}{2\omega_{\bar{D}^*}(\vec{q})} \frac{1}{P_{\text{in}}^0 - q^0 - \omega_{\bar{D}^*}(\vec{q}) + i\epsilon} i \frac{M_{\Sigma_c}}{E_{\Sigma_c}(\vec{q})} \frac{1}{K_{\text{in}}^0 + q^0 - E_{\Sigma_c}(\vec{q}) + i\epsilon}, \quad (13) \end{aligned}$$

$$\begin{aligned} -i\delta V^{PC} &= \int \frac{d^4q}{(2\pi)^4} \left(\frac{m_{D^*}}{m_{K^*}} \right)^2 g \left(\sqrt{2} \frac{2F}{2f_\pi} \vec{\sigma} \cdot \vec{\epsilon} \right) (-g) \left(2\sqrt{2}\vec{\epsilon} \cdot \vec{q} \frac{1}{q^{02} - \vec{q}^2 - m_\pi^2} \frac{2F}{2f_\pi} \vec{\sigma} \cdot \vec{q} \right) \\ &\quad \times i \frac{1}{2\omega_{\bar{D}^*}(\vec{q})} \frac{1}{P_{\text{in}}^0 - q^0 - \omega_{\bar{D}^*}(\vec{q}) + i\epsilon} i \frac{M_{\Sigma_c}}{E_{\Sigma_c}(\vec{q})} \frac{1}{K_{\text{in}}^0 + q^0 - E_{\Sigma_c}(\vec{q}) + i\epsilon}, \quad (14) \end{aligned}$$

$$\begin{aligned}
-i\delta V^{CC} = & \int \frac{d^4q}{(2\pi)^4} \left(\frac{m_{D^*}}{m_{K^*}} \right)^2 g \left(\sqrt{2} \frac{2F}{2f_\pi} \vec{\sigma} \cdot \vec{\epsilon} \right) (-g) \left(\sqrt{2} \frac{2F}{2f_\pi} \vec{\sigma} \cdot \vec{\epsilon} \right) \\
& \times i \frac{1}{2\omega_{\bar{D}^*}(\vec{q})} \frac{1}{P_{\text{in}}^0 - q^0 - \omega_{\bar{D}^*}(\vec{q}) + i\epsilon} i \frac{M_{\Sigma_c}}{E_{\Sigma_c}(\vec{q})} \frac{1}{K_{\text{in}}^0 + q^0 - E_{\Sigma_c}(\vec{q}) + i\epsilon}, \quad (15)
\end{aligned}$$

where P_{in}^0 and K_{in}^0 are the energies of the incoming meson \bar{D} and baryon Σ_c respectively, and $\omega_{\bar{D}^*}(\vec{q}) = \sqrt{\vec{q}^2 + m_{D^*}^2}$, etc., $E_{\Sigma_c}(\vec{q}) = \sqrt{\vec{q}^2 + m_{\Sigma_c}^2}$.

It is easy to handle the operators $\vec{\sigma}$ and $\vec{\epsilon}$ in the two pion exchange term of Eq. (13) for both cases of the $PB \rightarrow VB \rightarrow PB$ and $VB \rightarrow PB \rightarrow VB$ boxes. In the first case we can use the identity $(\vec{q} \cdot \vec{\sigma})^2 = \vec{q}^2$, and then the symmetric property in the integral

$$q_i q_j \rightarrow \frac{1}{3} \vec{q}^2 \delta_{ij} \quad (16)$$

and the summation of the polarization of the intermediate vector

$$\epsilon_i(\vec{q}) \epsilon_j(\vec{q}) = \delta_{ij}. \quad (17)$$

However, in the $VB \rightarrow PB \rightarrow VB$ box, the polarization vectors are external and there is no sum over polarizations, one is $\vec{\epsilon}$ and the other $\vec{\epsilon}'$. We still can use Eq. (16) and we obtain in both cases

$$\{(\vec{\sigma} \cdot \vec{q})(\vec{\epsilon} \cdot \vec{q})\}^2 \rightarrow \begin{cases} \vec{q}^4 & : PB \rightarrow VB \rightarrow PB \\ \frac{1}{3} \vec{q}^4 \vec{\epsilon} \cdot \vec{\epsilon}' & : VB \rightarrow PB \rightarrow VB \end{cases}. \quad (18)$$

From this result, the inverse box diagram, $\bar{D}^* \Sigma_c \rightarrow \bar{D} \Sigma_c \rightarrow \bar{D}^* \Sigma_c$, is found to have an extra factor $\frac{1}{3} \vec{\epsilon} \cdot \vec{\epsilon}'$. Furthermore, for the contributions which include the Kroll-Ruderman term, namely Eqs. (14) and (15), we use again Eq. (16) plus the property [25]

$$\langle PB | \vec{\sigma} \cdot \vec{\epsilon} | VB \rangle = \sqrt{3} \delta_{J,1/2}. \quad (19)$$

and we find in both cases that there is only $J = 1/2$ contribution and

$$(\vec{\sigma} \cdot \vec{\epsilon})(\vec{\sigma} \cdot \vec{q})(\vec{\epsilon} \cdot \vec{q}) = \vec{q}^2 \delta_{J,1/2}. \quad (20)$$

For other box diagrams involving $\Sigma_c \leftrightarrow \Lambda_c$ baryon conversion, one can obtain the potential in the same manner as done above. The final result is that we can use Eqs. (13)-(15), considering the appropriate masses or energies and making the following replacement

$$2 \left(\frac{2F}{2f} \right)^2 \rightarrow \left(\frac{2D}{2f} \right)^2. \quad (21)$$

Next, we evaluate the box diagrams of the sectors involving a baryon Σ_c^* . The two diagrams, $\bar{D} \Sigma_c \rightarrow \bar{D}^* \Sigma_c \rightarrow \bar{D} \Sigma_c$ and $\bar{D} \Sigma_c^* \rightarrow \bar{D}^* \Sigma_c^* \rightarrow \bar{D} \Sigma_c^*$, are different in their πBB vertices. The $\pi \Sigma_c^* \Sigma_c^*$ vertex is given by

$$-it_{\pi \Sigma_c^* \Sigma_c^*} = \frac{f_{\Sigma_c^*}}{m_\pi} \vec{S}_{\Sigma_c^*} \cdot \vec{q} T_{\Sigma_c^*}, \quad (22)$$

where $\vec{S}_{\Sigma_c^*}$ and $T_{\Sigma_c^*}$ represent a spin $S = 3/2$ and isospin $I = 1$ operator respectively. Using

the ordinary quark model, one finds

$$\frac{f_{\Sigma_c^*}}{m_\pi} = \frac{4}{5} \frac{f_{\pi NN}}{m_\pi} = \frac{4}{5} \frac{D+F}{2f}. \quad (23)$$

By counting the weight of each contribution in the same manner as for the case of Σ_c , we have the $\bar{D}\Sigma_c^* \rightarrow \bar{D}^*\Sigma_c^*$ transition amplitude

$$-it_{\bar{D}\Sigma_c^* \rightarrow \bar{D}^*\Sigma_c^*}^P = 2\sqrt{2}g \frac{m_{D^*}}{m_{K^*}} \vec{q} \cdot \vec{\epsilon} \frac{1}{q^2 - m_\pi^2} \frac{f_{\Sigma_c^*}}{m_\pi} \vec{S}_{\Sigma_c^*} \cdot \vec{q}. \quad (24)$$

A further simplification is done in this case and we evaluate the box for an average of the diagonal spin transition. We have

$$\frac{1}{4} \sum_{m, m'} \langle m' | \vec{S}_{\Sigma^*} \cdot \vec{q} | m \rangle \langle m | \vec{S}_{\Sigma^*} \cdot \vec{q} | m' \rangle = \frac{1}{4} q_i q_j \sum_{m, m'} \langle m' | S_{\Sigma^*} | m \rangle_i \langle m | S_{\Sigma^*} | m' \rangle_j. \quad (25)$$

Since there is no privileged direction after we sum over m, m' the matrix element, we have

$$\frac{1}{4} \sum_{m, m'} \langle m' | S_{\Sigma^*} | m \rangle_i \langle m | S_{\Sigma^*} | m' \rangle_j = A \delta_{ij}, \quad (26)$$

and by taking the trace, we obtain the spin factor $A = 5/4$. This allows us to write the following relationship

$$\left(\vec{S}_{\Sigma^*} \cdot \vec{q} \right) \left(\vec{S}_{\Sigma^*} \cdot \vec{q} \right) \rightarrow \frac{5}{4} \vec{q}^2. \quad (27)$$

Recalling the identity, $(\vec{\sigma} \cdot \vec{q})^2 = \vec{q}^2$ used in the case of spin 1/2 baryons in the intermediate states, in order to construct the box potential of the $\bar{D}\Sigma_c^* \rightarrow \bar{D}^*\Sigma_c^* \rightarrow \bar{D}\Sigma_c^*$, we implement the following substitution in Eqs. (13)-(15)

$$\left(\frac{2F}{2f} \right)^2 \rightarrow \frac{5}{4} \left(\frac{f_{\Sigma^*}}{m_\pi} \right)^2. \quad (28)$$

D. Contribution from the anomalous term

In addition to the VB and PB mixing term, another correction contributes to the \bar{D}^*B channels which does not interfere with the s -wave driving force at tree level. This contribution stems from the anomalous $\bar{D}^*\bar{D}^*\pi$ coupling and is taken into account in a box diagram too. By replacing the \bar{D} mesons in the PB - VB box by \bar{D}^* , we list down the possible cases for this anomalous box contribution

$$\begin{aligned} \bar{D}^*\Sigma_c &\rightarrow \bar{D}^*\Sigma_c \rightarrow \bar{D}^*\Sigma_c, \\ \bar{D}^*\Sigma_c &\rightarrow \bar{D}^*\Lambda_c \rightarrow \bar{D}^*\Sigma_c, \\ \bar{D}^*\Lambda_c &\rightarrow \bar{D}^*\Sigma_c \rightarrow \bar{D}^*\Lambda_c, \\ \bar{D}^*\Sigma_c^* &\rightarrow \bar{D}^*\Sigma_c^* \rightarrow \bar{D}^*\Sigma_c^*. \end{aligned}$$

One of them, the $\bar{D}^*\Sigma_c \rightarrow \bar{D}^*\Sigma_c \rightarrow \bar{D}^*\Sigma_c$ diagram, is depicted in Fig. 6.

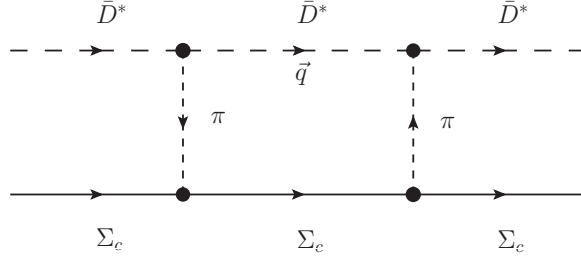


FIG. 6. Box diagram with anomalous $\bar{D}^* \bar{D}^* \pi$ vertex.

The anomalous $\bar{D}^* \bar{D}^* \pi$ vertex can be obtained from the Lagrangian ¹

$$\mathcal{L}_{VVP} = \frac{G'}{\sqrt{2}} \epsilon^{\mu\nu\alpha\beta} \langle \partial_\mu V_\nu \partial_\alpha V_\beta P \rangle, \quad (29)$$

with $G' = 3M_V^2/16\pi^2 f_\pi^3 (\simeq 14 \text{ GeV}^{-1})$ [39, 40] and the V and P matrices in $SU(4)$ are given in Ref. [41]. Thus, for the $\bar{D}^* \Sigma_c^* \rightarrow \bar{D}^* \Sigma_c^*$ transition amplitude we obtain

$$-it_{\bar{D}^* \Sigma_c^* \rightarrow \bar{D}^* \Sigma_c^*}^{\text{an}} = \frac{1}{2} 2\sqrt{2} \frac{G'}{\sqrt{2}} m_{D^*} \epsilon^{ijk} \epsilon_i(\vec{p}) q_j \epsilon_k(\vec{q}) \frac{2F}{2f_\pi} \frac{1}{q^2 - m_\pi^2} \vec{\sigma} \cdot \vec{q}, \quad (30)$$

with a four momentum of the incoming \bar{D}^* , $p^\mu \sim (m_{D^*}, \vec{0})$, and $\epsilon^{0\nu\alpha\beta} = \epsilon^{\nu\alpha\beta}$.

In the case of the anomalous term, there is no contact term. Here the box potential is obtained in analogy with the case of the previous box diagram, $\bar{D} \Sigma_c \rightarrow \bar{D}^* \Sigma_c \rightarrow \bar{D} \Sigma_c$. By using Eqs. (16) and (17), the operators of the intermediate states contract and lead to

$$[\epsilon^{ijk} \epsilon_i(\vec{p}) q_j \epsilon_k(\vec{q})]^2 = \vec{q}^2 \vec{\epsilon} \cdot \vec{\epsilon}' - (\vec{q} \cdot \vec{\epsilon})(\vec{q} \cdot \vec{\epsilon}') \rightarrow \frac{2}{3} \vec{q}^2 \vec{\epsilon} \cdot \vec{\epsilon}'. \quad (31)$$

This, together with $(\vec{\sigma} \cdot \vec{q})^2 = \vec{q}^2$ leads to a global factor $\frac{2}{3} \vec{q}^4 \vec{\epsilon} \cdot \vec{\epsilon}'$ instead of the factor $\frac{1}{3} \vec{q}^4 \vec{\epsilon} \cdot \vec{\epsilon}'$ that we had in Eq. (18) for the case of intermediate vectors.

III. FULL COUPLED CHANNELS CALCULATION

With an extension of the mixing effect between PB and VB channels caused by the pion exchange, we implement the full coupled channels calculation. Recalling the box potentials constructed in Sec. II C, we finally study the following four sectors separately.

$$\begin{aligned} J = 1/2 & : \bar{D} \Sigma_c, \bar{D}^* \Sigma_c, \bar{D}^* \Lambda_c \\ J = 3/2 & : \bar{D}^* \Sigma_c, \bar{D}^* \Lambda_c \\ J = 1/2 & : \bar{D}^* \Sigma_c^* \\ J = 3/2 & : \bar{D} \Sigma_c^*, \bar{D}^* \Sigma_c^* \end{aligned}$$

The driving force, the Weinberg-Tomozawa term, is already given in Sec. II A and it is found that these interactions have no off-diagonal interaction (see Tables A1 and A2). Furthermore

¹ An anomalous process, like the VVP interaction, is one that does not conserve “natural” parity. The “natural” parity of a particle is defined as follows: it is +1 if the particle transforms as a true tensor of that rank, and -1 if it transforms as a pseudotensor, e.g. π, γ, ρ and a_1 have “natural” parity -1, +1, +1 and -1, respectively.

the other interactions, the box diagrams from the local hidden gauge and the anomalous term, are added. Since a large mixture of VB and PB states would be expected from the results of Ref. [27], it is preferred to implement the full coupled channels calculation, especially between VB and PB channels which generate physical states or have attractive interaction. In this section, first we show the derivation of the effective transition potentials which allow us to implement the full coupled channels calculation, and subsequently the explicit form of the additional interactions to Weinberg-Tomozawa one are given. In Tables A5, A6, A7 and A8 of Appendix, the interactions for each sector are summarized.

A. Effective transition potential

We follow the scheme of the effective transition potential constructed in Ref. [27]. In this work, the generated states are looked for in the s -wave scattering amplitude, where the Weinberg-Tomozawa interaction appears. However, the intermediate states of the box potentials are not necessarily in the s -wave and then the box potentials should be decomposed into two parts to implement full coupled channels scheme. The part with intermediate states in the s -wave is utilized to construct the s -wave effective transition potential and the rest part is added to the Weinberg-Tomozawa interactions as a correction. On the other hand, since the anomalous $\bar{D}^* \bar{D}^* \pi$ coupling does not interfere with the Weinberg-Tomozawa term, these terms contribute only via the box diagram.

With the s -wave component of the $PB_a \rightarrow VB_b \rightarrow PB_a$ box potential, $\delta V_{PB_a \rightarrow VB_b \rightarrow PB_a}(s\text{-wave})$, such as $\bar{D}\Sigma_c \rightarrow \bar{D}^* \Lambda_c(s\text{-wave}) \rightarrow \bar{D}\Sigma_c$, we define an effective transition potential between PB_a and VB_b channels as

$$\tilde{V}_{\text{eff}}^2 G_{VB_b} = \delta V_{PB_a \rightarrow VB_b \rightarrow PB_a}(s\text{-wave}), \quad (32)$$

with G_{VB_b} being the G function of the intermediate VB_b channel. In the same manner, from the counterpart diagram, $VB_b \rightarrow PB_a \rightarrow VB_b$, we can also define the other $PB_a \leftrightarrow VB_b$ transition potential with a corresponding box potential $\delta V'$

$$\tilde{V}'^2_{\text{eff}} G_{PB_a} = \delta V'_{VB_b \rightarrow PB_a \rightarrow VB_b}(s\text{-wave}). \quad (33)$$

To ensure the symmetric property of the potential or the amplitude matrices, namely $V_{ij} = V_{ji}$, we define the effective transition potential by taking the average of the two potentials

$$V_{\text{eff}} = \frac{1}{2}(\tilde{V}_{\text{eff}} + \tilde{V}'_{\text{eff}}). \quad (34)$$

However, it turns out that the potentials are very similar and in fact they are identical in the limit of $m_D = m_{D^*}$ as demonstrated in Refs. [26, 27], hence, the concept of V_{eff} is well defined. From the definitions, \tilde{V}_{eff} and \tilde{V}'_{eff} are found to be double-valued functions. Therefore, the relative signs of the two functions should be taken equal not to be canceled out. We choose \tilde{V}_{eff} with negative real part as it corresponds to a virtual pion exchange. The energy of the generated states does not depend upon this prescription.

Among the relevant box diagrams, it is obvious that the term involving the contact term, Eqs. (14) and (15), contribute only to the s -wave due the product $\vec{\sigma} \cdot \vec{\epsilon}$. Therefore, the intermediate states of these terms are always in the s -wave. On the other hand, the case of the two pion exchange term is different. When the extraction of the s -wave component is

necessary, we utilize the following separation for each of the pion exchange

$$(\vec{\sigma} \cdot \vec{q})(\vec{\epsilon} \cdot \vec{q}) \rightarrow \epsilon_i q_i \sigma_j q_j = \epsilon_i \sigma_j \left\{ \frac{1}{3} q^2 \delta_{ij} + \left(q_i q_j - \frac{1}{3} q^2 \delta_{ij} \right) \right\}, \quad (35)$$

where the first term of the last expression of the equation corresponds to the s -wave component and the second to d -wave, and this separation leads to

$$\{(\vec{\sigma} \cdot \vec{q})(\vec{\epsilon} \cdot \vec{q})\}^2 (s\text{-wave}) \rightarrow \left\{ \begin{array}{l} \frac{1}{3} \vec{q}^4 \quad : \quad PB \rightarrow VB \rightarrow PB \\ \frac{1}{3} \frac{1}{3} \vec{q}^4 \vec{\epsilon} \cdot \vec{\epsilon}' \quad : \quad VB \rightarrow PB \rightarrow VB \end{array} \right. . \quad (36)$$

Subtracting the s -wave contribution from the total contribution of the box we obtain the d -wave contribution.

In the following sections, the explicit forms of the potentials are shown where the expressions of $I'_1, I'_2, I'_3, FAC, I_1, I_2,$ and I_3 can be seen in Eqs. (34)-(37) and (41)-(43) of Ref. [26].

1. $\bar{D}\Sigma_c, \bar{D}^*\Sigma_c, \bar{D}^*\Lambda_c$ with $J = 1/2$

In this sector, the VB intermediate states in the $PB \rightarrow VB \rightarrow PB$ box potentials can have s -wave and d -wave contributions. By using the decomposition, Eq. (36), and recalling that the contact-contact and contact-pion terms contribute to only the s -wave component, we can decompose them into two parts

$$\begin{aligned} \delta V_I(s\text{-wave}) &= \delta V (\bar{D}\Sigma_c \rightarrow \bar{D}^*\Sigma_c \rightarrow \bar{D}\Sigma_c; J = 1/2, s\text{-wave}) \\ &= REL1 \times FAC \times \left(\frac{1}{3} \frac{\partial I_1}{\partial m_\pi^2} + 2I_2 + I_3 \right), \end{aligned} \quad (37)$$

$$\begin{aligned} \delta V_{II}(s\text{-wave}) &= \delta V (\bar{D}\Sigma_c \rightarrow \bar{D}^*\Lambda_c \rightarrow \bar{D}\Sigma_c; J = 1/2, s\text{-wave}) \\ &= REL2 \times FAC \times \left(\frac{1}{3} \frac{\partial I_1}{\partial m_\pi^2} + 2I_2 + I_3 \right), \end{aligned} \quad (38)$$

$$\delta V (\bar{D}\Sigma_c \rightarrow \bar{D}^*\Sigma_c \rightarrow \bar{D}\Sigma_c; J = 1/2, d\text{-wave}) = REL1 \times FAC \times \frac{2}{3} \frac{\partial I_1}{\partial m_\pi^2}, \quad (39)$$

$$\delta V (\bar{D}\Sigma_c \rightarrow \bar{D}^*\Lambda_c \rightarrow \bar{D}\Sigma_c; J = 1/2, d\text{-wave}) = REL2 \times FAC \times \frac{2}{3} \frac{\partial I_1}{\partial m_\pi^2}, \quad (40)$$

where we use the factor FAC together with the relative factors as discussed in Sec. IIC

$$FAC = \frac{9}{2} g^2 \left(\frac{m_{D^*}}{m_{K^*}} \right)^2 \left(\frac{F+D}{2f} \right)^2, \quad (41)$$

$$REL1 = \frac{4}{9} \left(\frac{2F}{D+F} \right)^2, \quad (42)$$

$$REL2 = \frac{1}{9} \left(\frac{2D}{D+F} \right)^2. \quad (43)$$

The PB intermediate states in the $VB \rightarrow PB \rightarrow VB$ box potentials are necessarily in

the s -wave and thus with Eqs. (18), (42) and (43) we have

$$\begin{aligned}\delta V'_I(s\text{-wave}) &= \delta V (\bar{D}^*\Sigma_c \rightarrow \bar{D}\Sigma_c \rightarrow \bar{D}^*\Sigma_c; J = 1/2) \\ &= REL1 \times FAC \times \left(\frac{\partial I'_1}{\partial m_\pi^2} + 2I'_2 + I'_3 \right),\end{aligned}\quad (44)$$

$$\begin{aligned}\delta V'_{II}(s\text{-wave}) &= \delta V (\bar{D}^*\Lambda_c \rightarrow \bar{D}\Sigma_c \rightarrow \bar{D}^*\Lambda_c; J = 1/2) \\ &= REL2 \times FAC \times \left(\frac{\partial I'_1}{\partial m_\pi^2} + 2I'_2 + I'_3 \right).\end{aligned}\quad (45)$$

From the s -wave box potentials given by Eqs. (37) and (44) and by Eqs. (38) and (45), we construct the following two effective transition potentials

$$V_{\bar{D}\Sigma_c \leftrightarrow \bar{D}^*\Sigma_c}^{\text{eff}} = \frac{\sqrt{\delta V_I(s\text{-wave})/G_{\bar{D}^*\Sigma_c}} + \sqrt{\delta V'_I(s\text{-wave})/G_{\bar{D}\Sigma_c}}}{2},\quad (46)$$

$$V_{\bar{D}\Sigma_c \leftrightarrow \bar{D}^*\Lambda_c}^{\text{eff}} = \frac{\sqrt{\delta V_{II}(s\text{-wave})/G_{\bar{D}^*\Lambda_c}} + \sqrt{\delta V'_{II}(s\text{-wave})/G_{\bar{D}\Sigma_c}}}{2}.\quad (47)$$

They are placed in the corresponding off-diagonal channels.

Furthermore, as discussed before, the $\bar{D}\Lambda_c$ contribution is just added to the $\bar{D}^*\Sigma_c$ channel as a box correction,

$$\delta V (\bar{D}^*\Sigma_c \rightarrow \bar{D}\Lambda_c \rightarrow \bar{D}^*\Sigma_c; J = 1/2) = REL2 \times FAC \times \left(\frac{\partial I'_1}{\partial m_\pi^2} + 2I'_2 + I'_3 \right).\quad (48)$$

We also show the box potentials which stem from the anomalous term

$$\delta V_{\text{an}} (\bar{D}^*\Sigma_c \rightarrow \bar{D}^*\Sigma_c \rightarrow \bar{D}^*\Sigma_c) = REL1 \times AFAC \times \frac{\partial I'_1}{\partial m_\pi^2},\quad (49)$$

$$\delta V_{\text{an}} (\bar{D}^*\Sigma_c \rightarrow \bar{D}^*\Lambda_c \rightarrow \bar{D}^*\Sigma_c) = REL2 \times AFAC \times \frac{\partial I'_1}{\partial m_\pi^2},\quad (50)$$

$$\delta V_{\text{an}} (\bar{D}^*\Lambda_c \rightarrow \bar{D}^*\Sigma_c \rightarrow \bar{D}^*\Lambda_c) = REL2 \times AFAC \times \frac{\partial I'_1}{\partial m_\pi^2},\quad (51)$$

with a factor which comes from Eqs. (30) and (31)

$$AFAC = \frac{9}{8}G'^2 \left(\frac{D+F}{2f} \right)^2 m_{D^*}^2.\quad (52)$$

These box potentials are added to the $\bar{D}^*\Sigma_c$ and $\bar{D}^*\Lambda_c$ diagonal Weinberg-Tomozawa interaction equally in the $J = 1/2$ and $J = 3/2$ sectors.

2. $\bar{D}^*\Sigma_c, \bar{D}^*\Lambda_c$ with $J = 3/2$

Since the PB intermediate states with $J = 3/2$ are automatically in the d -wave, we just add the following box diagram potentials to the diagonal interactions

$$\delta V (\bar{D}^*\Sigma_c \rightarrow \bar{D}\Sigma_c \rightarrow \bar{D}^*\Sigma_c; J = 3/2) = REL1 \times FAC \times \frac{\partial I'_1}{\partial m_\pi^2}, \quad (53)$$

$$\delta V (\bar{D}^*\Lambda_c \rightarrow \bar{D}\Sigma_c \rightarrow \bar{D}^*\Lambda_c; J = 3/2) = REL2 \times FAC \times \frac{\partial I'_1}{\partial m_\pi^2}, \quad (54)$$

$$\delta V (\bar{D}^*\Sigma_c \rightarrow \bar{D}\Lambda_c \rightarrow \bar{D}^*\Sigma_c; J = 3/2) = REL2 \times FAC \times \frac{\partial I'_1}{\partial m_\pi^2}. \quad (55)$$

Remember that the box potentials from the anomalous term, Eqs. (49)-(51), are also added to this sector. Note that in this sector there is no transition between the $\bar{D}^*\Sigma_c$ and $\bar{D}^*\Lambda_c$ channels and hence, in this sector we do not have coupled channels but two single channels.

3. $\bar{D}^*\Sigma_c^*$ with $J = 1/2, 5/2$

In this sector, we have only a $\bar{D}^*\Sigma_c^*$ channel. Considering that the $\bar{D}\Sigma_c^*$ channel with $J = 1/2, 5/2$ can not be in the s -wave, we find that the box potentials should include only the pion-pion term with Eq. (18). Taking into account Eq. (28), we have the $\bar{D}^*\Sigma_c^* \rightarrow \bar{D}\Sigma_c^* \rightarrow \bar{D}^*\Sigma_c^*$ box diagram

$$\delta V (\bar{D}^*\Sigma_c^* \rightarrow \bar{D}\Sigma_c^* \rightarrow \bar{D}^*\Sigma_c^*; J = 1/2) = REL3 \times FAC \times \frac{\partial I'_1}{\partial m_\pi^2}, \quad (56)$$

with

$$REL3 = \frac{5}{9} \left(\frac{f_{\Sigma^*}}{m_\pi} \right)^2 / \left(\frac{D+F}{2f} \right)^2 = \frac{16}{45}. \quad (57)$$

This is just added to the $\bar{D}^*\Sigma_c^*$ diagonal Weinberg-Tomozawa interaction with the extra contribution from the anomalous term

$$\delta V_{\text{an}} (\bar{D}^*\Sigma_c^* \rightarrow \bar{D}^*\Sigma_c^* \rightarrow \bar{D}^*\Sigma_c^*) = REL3 \times AFAC \times \frac{\partial I'_1}{\partial m_\pi^2}. \quad (58)$$

4. $\bar{D}\Sigma_c^*$ and $\bar{D}^*\Sigma_c^*$ with $J = 3/2$

We here consider the $\bar{D}\Sigma_c^*$ and $\bar{D}^*\Sigma_c^*$ coupled channels. The $\bar{D}\Sigma_c^*$ intermediate state with $J = 3/2$ has an admixture of the s -wave and d -wave components and thus each potential is separated into s - and d -wave contributions as done in the $PB-VB$ sector with $J = 1/2$

$$\begin{aligned} \delta V'_{III}(s\text{-wave}) &= \delta V (\bar{D}^*\Sigma_c^* \rightarrow \bar{D}\Sigma_c^* \rightarrow \bar{D}^*\Sigma_c^*; J = 3/2, s\text{-wave}) \\ &= REL3 \times FAC \times \left(\frac{1}{3} \frac{\partial I'_1}{\partial m_\pi^2} + 2I'_2 + I'_3 \right), \end{aligned} \quad (59)$$

and

$$\delta V (\bar{D}^*\Sigma_c^* \rightarrow \bar{D}\Sigma_c^* \rightarrow \bar{D}^*\Sigma_c^*; J = 3/2, d\text{-wave}) = REL3 \times FAC \times \frac{2}{3} \frac{\partial I_1'}{\partial m_\pi^2}. \quad (60)$$

On the other hand, although the $\bar{D}^*\Sigma_c^*$ intermediate state of the $\bar{D}\Sigma_c^* \rightarrow \bar{D}^*\Sigma_c^* \rightarrow \bar{D}\Sigma_c^*$ box diagram also has the s -wave component, the many spin contributions of $\bar{D}^*\Sigma_c^*$ complicate the analysis. Therefore, we adopt only the definition of Eq. (33) instead of Eq. (34) to construct the $\bar{D}\Sigma_c^* \leftrightarrow \bar{D}^*\Sigma_c^*$ effective transition potential

$$V_{\bar{D}\Sigma_c^* \leftrightarrow \bar{D}^*\Sigma_c^*}^{\text{eff}} = \sqrt{\delta V'_{III}(s\text{-wave})/G_{\bar{D}\Sigma_c^*}}, \quad (61)$$

and by using this effective potential, we extract the s -wave contribution from the total $\bar{D}\Sigma_c^* \rightarrow \bar{D}^*\Sigma_c^* \rightarrow \bar{D}\Sigma_c^*$ box

$$\begin{aligned} & \delta V (\bar{D}\Sigma_c^* \rightarrow \bar{D}^*\Sigma_c^* \rightarrow \bar{D}\Sigma_c^*; J = 3/2, \text{except } s\text{-wave}) \\ &= REL3 \times FAC \times \left(\frac{\partial I_1}{\partial m_\pi^2} + 2I_2 + I_3 \right) - \left(V_{\bar{D}\Sigma_c^* \leftrightarrow \bar{D}^*\Sigma_c^*}^{\text{eff}} \right)^2 G_{\bar{D}^*\Sigma_c^*}. \end{aligned} \quad (62)$$

We also add the potential from the anomalous term, Eq. (58), to the $\bar{D}^*\Sigma_c^*$ channel.

B. Resonance measured on the real axis

In the full coupled channels scheme, we would see the generation of several physical states. Under the coupled channels unitary scheme, the corresponding poles are looked for in the second Riemann sheet in the complex plane. In the case of bound states, poles appear on the real axis below the threshold in the first Riemann sheet and thus we look for the bound states poles as usual. From the residue of the scattering amplitude at the pole, M_R , we obtain the coupling constant g_i, g_j

$$g_i g_j = \lim_{\sqrt{s} \rightarrow M_R} (\sqrt{s} - M_R) T_{ij}(\sqrt{s}). \quad (63)$$

With the coupling constant and the G function at the bound state pole, we evaluate the wave function at the origin of channel i as $g_i G_i(M_R)$ [29].

Resonance poles, on the other hand, emerge in the complex energy plane. As we do not know how to extend the box potentials or effective potentials to the complex energy plane, we analyze the resonance states in another way. Instead of looking for a pole position of the scattering amplitude, we search a peak position M_R on the real axis, where the square of the magnitude of the amplitude $|T(\sqrt{s})|^2$ has a maximum. Since this position is not exactly the same between different scattering channels, we determine it in the dominant channel. Together with the peak position, we measure the width of the state, Γ_R , on the real axis as being a distance between two points where $|T(\sqrt{s})|^2$ has a half maximum value.

Next, we determine the coupling constants of resonance states with the measured mass and width. On the real axis and in the vicinity of the peak position, we assume the Breit-Wigner amplitude

$$T_{ij}(\sqrt{s}) \sim \frac{g_i g_j}{\sqrt{s} - M_R + i\Gamma_R/2}. \quad (64)$$

At the peak position, the coupling constants of the dominant channel d is given by the imaginary part of the amplitude

$$\text{Im}T_{ij}(M_R) = -\frac{g_i g_j}{\Gamma_R/2}, \quad g_d = \sqrt{\left| \frac{\Gamma_R}{2} \text{Im}T_{dd}(M_R) \right|}, \quad (65)$$

where g_d is taken as a positive number. In order not to lose the relative signs, the coupling constants of the other channels are determined from the ratio of the imaginary part of the amplitude in different channels

$$g_i = \frac{\text{Im}T_{id}(M_R)}{\text{Im}T_{dd}(M_R)} g_d. \quad (66)$$

The wave function at the origin, or the probability, can be obtained from the coupling constant and the G function at the pole position. In this case, since we determine the coupling at the peak position, for the sake of consistency we evaluate the wave function at the origin of channel i as $g_i G_i(M_R)$.

IV. NUMERICAL RESULTS OF THE FULL COUPLED CHANNELS CALCULATION

In this section, we show the results of the full coupled channels approach. In order to obtain the numerical results, we take three cut off parameters, q_{max}^P in the pseudoscalar-baryon loop, q_{max}^V in the vector-baryon loop and q_{max}^B in the box diagrams. Since no nucleon resonance state in the high energy region of our interest has been reported, we tentatively adopt the cut off parameters used in the previous work of open charm baryons [27] where the parameters were chosen to reproduce two Λ_c resonances, $\Lambda_c(2592)$ and $\Lambda_c(2625)$. In Table I, three sets of three cut off parameters are listed. Furthermore, as well as in the previous work, we put the Yukawa form factor, $F(\vec{q}) = \Lambda^2/(\Lambda^2 + \vec{q}^2)$, on the $\pi BB'$ vertices in all the box diagrams, with cut off $\Lambda = 1000$ MeV, a standard value. In the following subsections, we show the results of the $\bar{D}\Sigma_c$ and $\bar{D}^*\Sigma_c$ states and $\bar{D}\Sigma_c^*$ and $\bar{D}^*\Sigma_c^*$ states separately.

	set I	set II	set III
q_{max}^B	600	800	1000
q_{max}^V	771	737	715
q_{max}^P	527	500	483

TABLE I. Cut off parameters, q_{max}^V (q_{max}^P) for the vector-baryon (pseudoscalar-baryon) G function, q_{max}^B for all the box potentials.

A. $\bar{D}\Sigma_c$ and $\bar{D}^*\Sigma_c$ states

In Table II, the peak positions and the widths of the resonant states with $J = 1/2$, generated by the coupled channels of $\bar{D}\Sigma_c$, $\bar{D}^*\Sigma_c$ and $\bar{D}^*\Lambda_c$ with $\bar{D}\Lambda_c$ box diagrams, are

listed. As discussed in Sec. III B, in this work, we extract the nature of the resonant states not by looking for the corresponding poles in the complex energy plane but by measuring the scattering amplitude on the real axis. We determine the peak position and width of generated states from the $\bar{D}^*\Sigma_c \rightarrow \bar{D}^*\Sigma_c$ scattering amplitude.

We obtain two different narrow resonances. With the ambiguities from the choice of the cut off parameters, the lower energy state appears around $4228 \text{ MeV} \pm 15 \text{ MeV}$ with about 20 MeV width, while the higher energy state is very close to the $\bar{D}\Lambda_c$ threshold, 4295 MeV with 10 MeV width. The coupling constants g_i and the wave functions at the origin $g_i G_i$ for the middle set of the cut off parameters, obtained from Eqs. (65) and (66), are listed in Table III. From these wave functions, it is found that two states appear as two orthogonal states roughly as $\frac{1}{\sqrt{2}}(\bar{D}\Sigma_c \pm \bar{D}^*\Sigma_c)$. This situation is similar to the one observed in Ref. [27] where the $\frac{1}{\sqrt{2}}(DN - D^*N)$ corresponded to the $\Lambda_c(2595)$, while there was a prediction for an orthogonal state about $\frac{1}{\sqrt{2}}(DN + D^*N)$ which was much less bound ². This feature was also observed in Ref. [21] where the higher energy state appears with zero binding [42].

It is also remarkable that for both orthogonal states, the $\bar{D}^*\Sigma_c$ component has a bit stronger coupling than the $\bar{D}\Sigma_c$ component. This could be one of the consequence of the heavy quark limit. Although, even in the charm sector, the mass difference between D and D^* , $m_{D^*} - m_D \sim 140 \text{ MeV}$ is not so small yet, the vector-baryon system binds more than the pseudoscalar-baryon due to the anomalous term contributions and this mechanism makes it possible that the vector-baryon and pseudoscalar-baryon systems couple easier.

	set I	set II	set III
peak 1	4241.7	4227.6	4218.6
width 1	19.5	21.1	21.5
peak 2	4296.8	4295.1	4294.5
width 2	13.1	10.6	9.6

TABLE II. Peak positions and their widths in the full coupled channels of $\bar{D}\Sigma_c[4321]$, $\bar{D}^*\Sigma_c[4462]$, $\bar{D}^*\Lambda_c[4295]$ with $J = 1/2$ measured in the $\bar{D}^*\Sigma_c \rightarrow \bar{D}^*\Sigma_c$ channel as a function of $q_{\text{max}}^{B,V,P}$. (The number in brackets after the channel indicates the threshold mass of the channel. Units: MeV)

(4227.6, 21.1)	$\bar{D}\Sigma_c$	$\bar{D}^*\Sigma_c$	$\bar{D}^*\Lambda_c$
g_i	4.40	5.39	0.39
$g_i G_i$	-15.66	-24.17	-3.31
(4295.1, 10.6)	$\bar{D}\Sigma_c$	$\bar{D}^*\Sigma_c$	$\bar{D}^*\Lambda_c$
g_i	-1.27	2.28	-0.11
$g_i G_i$	8.46	-12.60	$2.09 + i0.04$

TABLE III. The coupling constants to various channels for the poles in the $J = 1/2$ sector of $\bar{D}^*\Sigma_c$ and coupled channels, taking the cutoff Set II of Table I.

² In Ref. [27] the sign of V_{eff} was taken positive and here we take it negative. The energies do not depend upon this prescription but the $\frac{1}{\sqrt{2}}(DN \pm D^*N)$ combination would correspond now to $\frac{1}{\sqrt{2}}(DN \mp D^*N)$.

Next we see the $\bar{D}^*\Sigma_c$ and $\bar{D}^*\Lambda_c$ single channels with $J = 3/2$. As expected, the $\bar{D}^*\Lambda_c$ channel generates no state and we observe the $\bar{D}^*\Sigma_c$ broad resonance whose mass is 4217 MeV and width is around 100 MeV as listed in Table IV. This resonance is generated below the $\bar{D}\Sigma_c^*$ threshold but can decay into $\bar{D}\Lambda_c$ via the pion exchange, as well as the two resonance states with $J = 1/2$. Compared to $J = 1/2$ resonances, this $J = 3/2$ resonance is much broader because of the difference of the $\bar{D}^*\Sigma_c \rightarrow \bar{D}\Lambda_c \rightarrow \bar{D}^*\Sigma_c$ box diagram as seen in Eqs. (45) and (55).

Apart from masses or widths of the generated states, it is remarkable the similarity between the results of the hidden and open charm baryon. The vector-baryon system whose interaction is attractive, such as in $\bar{D}^*\Sigma_c$ or D^*N , generate deeply bound states with $J = 1/2$ and $J = 3/2$ and the pion exchange removes their spin degeneracies. On the other hand, the corresponding pseudoscalar-baryon system such as $\bar{D}\Sigma_c$ or DN generates shallow-bound states with $J = 1/2$. As a consequence, in the $J = 1/2$ sector, a pair of orthogonal states emerges as a mixture of VB and PB bound states, while in the $J = 3/2$ sector one deeply (quasi-)bound state is generated.

	set I	set II	set III
peak	4250.5	4217.7	4205.8
width	140.8	103.2	82.0

TABLE IV. Peak positions and their widths in the $\bar{D}^*\Sigma_c[4462]$ single channel with $J = 3/2$ sector as a function of $q_{\max}^{B,V,P}$. (Units: MeV)

We come back here to the results of Refs. [3, 4] and admit an extra width of about 30 MeV for the two lower $\frac{1}{\sqrt{2}}(\bar{D}^*\Sigma_c \pm \bar{D}\Sigma_c)$ states from the coupling to the light PB or VB sectors.

B. $\bar{D}\Sigma_c^*$ and $\bar{D}^*\Sigma_c^*$ states

In this subsection we show the results of the generated states involving $\bar{D}\Sigma_c^*$ and $\bar{D}^*\Sigma_c^*$ channels. In these sectors, bound states are developed and then we look for the corresponding poles as discussed in Sec. III B. In Table V, the pole positions of states generated by the $\bar{D}^*\Sigma_c^*$ single channel with $J = 1/2, 5/2$ are listed. We obtain a $\bar{D}^*\Sigma_c^*$ bound state with an energy 4344 with 10 MeV uncertainty from the cutoff setup, which appears around 180 MeV below the $\bar{D}^*\Sigma_c^*$ threshold.

	set I	set II	set III
Pole	4354.5	4344.1	4337.5

TABLE V. Poles in the $\bar{D}^*\Sigma_c^*[4527]$ single channel with $J = 1/2, 5/2$ as a function of cut off $q_{\max}^{B,V,P}$. (Units: MeV)

Next we see the results of coupled channels of $\bar{D}\Sigma_c^*$ and $\bar{D}^*\Sigma_c^*$ with $J = 3/2$. The pole positions of the generated states are listed in Table VI. In this sector, we obtain two bound states which are not far from the $\bar{D}^*\Sigma_c^*$ bound states with $J = 1/2$. The two states

are separated by about 50 MeV and the higher state appears a few MeV below the $\bar{D}\Sigma_c^*$ threshold. We show the coupling constants and the wave functions at the origin with the cut off set II in Table VII. From these wave functions, it is found that two bound states are the mixture of $\bar{D}\Sigma_c^*$ and $\bar{D}^*\Sigma_c^*$ corresponding roughly to the $\frac{1}{\sqrt{2}}(\bar{D}\Sigma_c^* \pm \bar{D}^*\Sigma_c^*)$ combinations.

	set I	set II	set III
Pole 1	4330.6	4324.9	4319.9
Pole 2	4384.1	4377.8	4374.4

TABLE VI. Poles in coupled channels of $\bar{D}\Sigma_c^*[4385]$, $\bar{D}^*\Sigma_c^*[4527]$ with $J = 3/2$ as a function of $q_{\max}^{B,V,P}$. (Units: MeV)

4324.85	$\bar{D}\Sigma_c^*$	$\bar{D}^*\Sigma_c^*$
g_i	3.61	4.89
$g_i G_i^{II}$	-16.54	-24.22
4378.84	$\bar{D}\Sigma_c^*$	$\bar{D}^*\Sigma_c^*$
g_i	-1.25	3.00
$g_i G_i^{II}$	12.30	-17.57

TABLE VII. The coupling constants to various channels for the poles in the $J = 3/2$ sector of $\bar{D}\Sigma_c^*$, $\bar{D}^*\Sigma_c^*$, taking the cutoff Set II of Table I.

V. SUMMARY AND CONCLUSIONS

In this work, the dynamics of an anti-charmed meson and a charmed baryon is studied in order to investigate the hidden charm resonances with isospin $I = 1/2$, N^* , in the energy region around 4200 \sim 4400 MeV. Since all the hadronic particles of our interest contain the charm quark, the extended local hidden gauge approach with SU(4) symmetry, as studied in Refs. [1, 2, 4], is employed to extract the information of the relevant vertices. Consequently, the leading interaction proceeds via the vector exchange and results in the Weinberg-Tomozawa interaction. Furthermore, we also take into account two types of additional interactions, as a box diagram correction. One of them with the $\bar{D}\bar{D}^*\pi$ vertex from the local hidden gauge scheme, proceeds via the pion exchange and requires the corresponding contact term. The other one comes from the anomalous $\bar{D}^*\bar{D}^*\pi$ interaction. The former additional interaction allows the PB and VB sectors to couple to each other. As pointed out in the previous works, we also place high importance on this mixing effect. Hence we have solved the Bethe-Salpeter equation under the full coupled channels scheme by constructing the effective transition potential following the discussion of Ref. [27]. The particular values of the πBB vertices, allowed us to classify the states into four sectors of the hidden charm systems, $\bar{D}\Sigma_c, \bar{D}^*\Sigma_c^*, \bar{D}^*\Lambda_c$ with $J = 1/2$, $\bar{D}^*\Sigma_c, \bar{D}^*\Lambda_c^*$ with $J = 3/2$, $\bar{D}^*\Sigma_c^*$ with $J = 1/2$ and $\bar{D}\Sigma_c^*, \bar{D}^*\Sigma_c^*$ with $J = 3/2$.

By looking for the bound state poles and measuring the resonant peaks on the real axis, as discussed in Sec. III B, we have seen that six states appear with several angular momenta.

Furthermore, from the wave function at the origin, the dominant components of the states have been evaluated. The properties of the states, masses, widths, dominant components and main decay channel, are summarized in Table VIII.

main channel	J	(E, Γ) [MeV]	main decay channels
$\frac{1}{\sqrt{2}}(\bar{D}^*\Sigma_c + \bar{D}\Sigma_c)$	1/2	4228, 21(51)	$\bar{D}\Lambda_c$
$\frac{1}{\sqrt{2}}(\bar{D}^*\Sigma_c - \bar{D}\Sigma_c)$	1/2	4295, 11(41)	$\bar{D}\Lambda_c$
$\bar{D}^*\Sigma_c$	3/2	4218, 103	$\bar{D}\Lambda_c$
$\bar{D}^*\Sigma_c^*$	1/2, 5/2	4344, 0	—
$\frac{1}{\sqrt{2}}(\bar{D}^*\Sigma_c^* + \bar{D}\Sigma_c^*)$	3/2	4325, 0	—
$\frac{1}{\sqrt{2}}(\bar{D}^*\Sigma_c^* - \bar{D}\Sigma_c^*)$	3/2	4378, 0	—

TABLE VIII. Energies and widths of the obtained states with the dominant component and main decay channels of each state. All the states are nucleon resonances with negative parity and have an estimated uncertainty of ± 20 MeV. The numbers in brackets for the first two states correspond to the estimated width, adding the 30 MeV width obtained in Refs. [3, 4] from coupling to the light PB or VB sectors.

The three generated states with Σ_c are, a pair of orthogonal states with $J = 1/2$, $\frac{1}{\sqrt{2}}(\bar{D}^*\Sigma_c \pm \bar{D}\Sigma_c)$, and, a resonance dominated by the $\bar{D}^*\Sigma_c$ component with $J = 3/2$. The two orthogonal states with energies around 4228 and 4295 MeV respectively, differ from each other by about 65 MeV and have a small width due to the weak coupling to the $\bar{D}\Lambda_c$. On the other hand, the $\bar{D}^*\Sigma_c$ state with $J = 3/2$ emerges around 4218 MeV with a large width 103 MeV. It is instructive to see the similarity in the generated states with Σ_c^* . Around 100 MeV above the region of the three state of Σ_c , a pair of the orthogonal states with $J = 3/2$, $\frac{1}{\sqrt{2}}(\bar{D}^*\Sigma_c^* \pm \bar{D}\Sigma_c^*)$ and one spin degenerate state with $J = 1/2, 5/2$ of $\bar{D}^*\Sigma_c^*$ develop. Considering the mass difference between Σ_c and Σ_c^* , $M_{\Sigma_c^*} - M_{\Sigma_c} \sim 65$ MeV, this result might indicate the realization of the heavy quark spin symmetry regarding the charmed baryon pair, Σ_c and Σ_c^* .

In the end, let us discuss the result comparing them to those of Refs. [1, 2, 4]. Apart from the use of the different cutoff parameters and the neglect of the light hadron sectors that simply give the width to the generated states, we employ the same interactions for the PB and VB sectors respectively. In Ref. [4], the PB sectors with the same quantum number develop physical states around 4250 MeV, not so far away from our results, however, the VB states appear much higher than ours, about 200 MeV higher. This is also the case in the work done in Ref. [43] done along the same lines.

In all these works [1, 2, 4], the box diagrams were not considered and the PB and VB sectors were studied independently. We have seen in the present work that due to the pion exchange that induces PB and VB mixing, the VB states get much bound. In addition, the pion exchange in the anomalous sector, which is only operative for the VB sector, provides a further contribution to the VB binding.

Another work that deserves attention in this discussion is the one of Ref. [23]. There a unitarized coupled channel approach, also mixing PB and VB states is done. The authors

use the Weinberg-Tomozawa interaction as leading contribution and an extended SU(8) spin-flavour symmetry constraint, with modifications implemented to respect HQSS. They obtain also bound states but the energies are almost 200 MeV smaller than what we find in the present work.

There are other calculations based on the quark model [44]. The authors also find bound states for different spins, and the energies range between 3900 \sim 4500 MeV. One should note that in this latter work, the predictions differ by about, 200 \sim 300 MeV depending on the interaction used, a color magnetic interaction in one case and a chiral interaction in the other. A detailed discussion of these different model is done in Ref. [42].

The comparison of the results obtained here with those of other works is instructive and indicate the large uncertainties in the predictions in this sector. In this respect, one should mention an earlier work where states are found with a binding of 1000 MeV [45], which, as discussed in Ref. [4], is somewhat extreme. These large theoretical differences contrast with the situation in other sectors, like the one of open charm, where the constraints of reproducing existing experimental data makes the predictions of different approaches more similar. Yet, one thing is shared by all these approaches and this is the existence of many bound states of the N^* type.

The former discussion should be sufficient incentive to search for these states, which would bring a clear evidence of exotic baryonic states, with a quark structure significantly different from the standard one of the baryons made up of three quarks.

ACKNOWLEDGMENTS

This work is partly supported by the Spanish Ministerio de Economía y Competitividad and European FEDER funds under Contract No. FIS2011-28853-C02-01 and the Generalitat Valenciana in the program Prometeo, 2009/090. We acknowledge the support of the European Community-Research Infrastructure Integrating Activity Study of Strongly Interacting Matter (Hadron Physics 3, Grant No. 283286) under the Seventh Framework Programme of the European Union. This work is also partly supported by the National Natural Science Foundation of China under Grant No. 11165005.

APPENDIX: SUMMARY OF THE INTERACTION

In this appendix we write the C_{ij} coefficients of Eq. (1) for the different channels.

C_{ij}	$\bar{D}\Sigma_c$
$\bar{D}\Sigma_c$	1

TABLE A1. C_{ij} coefficients for $\bar{D}\Sigma_c$ with $I = 1/2$ and $J^P = 1/2^-$.

C_{ij}	$\bar{D}^*\Sigma_c$	$\bar{D}^*\Lambda_c$
$\bar{D}^*\Sigma_c$	1	0
$\bar{D}^*\Lambda_c$		-1

TABLE A2. C_{ij} coefficients for $\bar{D}^*\Sigma_c$ and $\bar{D}^*\Lambda_c$ with $I = 1/2$ and $J^P = 1/2^-, 3/2^-$.

C_{ij}	$\bar{D}\Sigma_c^*$
$\bar{D}\Sigma_c^*$	1

TABLE A3. C_{ij} coefficients for $\bar{D}\Sigma_c^*$ with $I = 1/2$ and $J^P = 3/2^-$.

C_{ij}	$\bar{D}^*\Sigma_c^*$
$\bar{D}^*\Sigma_c^*$	1

TABLE A4. C_{ij} coefficients for $\bar{D}^*\Sigma_c^*$ with $I = 1/2$ and $J^P = 1/2^-, 3/2^-, 5/2^-$.

	$\bar{D}\Sigma_c$	$\bar{D}^*\Sigma_c$	$\bar{D}^*\Lambda_c$
$\bar{D}\Sigma_c$	Eqs. { (1) + (39) + (40) }	Eq. (46)	Eq. (47)
$\bar{D}^*\Sigma_c$		Eqs. { (1) + (48) + (49) + (50) }	0
$\bar{D}^*\Lambda_c$			Eqs. {(1) + (51) }

TABLE A5. Interactions in the coupled channels $\bar{D}\Sigma_c, \bar{D}^*\Sigma_c, \bar{D}^*\Lambda_c$ with $J^P = 1/2^-$.

	$\bar{D}^*\Sigma_c$	$\bar{D}^*\Lambda_c$
$\bar{D}^*\Sigma_c$	Eqs. { (1) + (53) + (55) + (49) + (50) }	0
$\bar{D}^*\Lambda_c$		Eqs. { (1) + (54) + (51) }

TABLE A6. Interactions in the two single channels $\bar{D}^*\Sigma_c, \bar{D}^*\Lambda_c$ with $J^P = 3/2^-$.

	$\bar{D}^*\Sigma_c^*$
$\bar{D}^*\Sigma_c^*$	Eqs. { (1) + (56) + (58) }

TABLE A7. Interactions in the single channel $\bar{D}^*\Sigma_c^*$ with $J^P = 1/2^-, 5/2^-$.

	$\bar{D}\Sigma_c^*$	$\bar{D}^*\Sigma_c^*$
$\bar{D}\Sigma_c^*$	Eqs. { (1) + (62) }	Eq. (61)
$\bar{D}^*\Sigma_c^*$		Eqs. { (1) + (60) + (58) }

TABLE A8. Interactions in the coupled channels $\bar{D}\Sigma_c^*, \bar{D}^*\Sigma_c^*$ with $J^P = 3/2^-$.

-
- [1] C. W. Xiao, J. Nieves and E. Oset, Phys. Rev. D **88**, 056012 (2013) [arXiv:1304.5368 [hep-ph]].
- [2] C. W. Xiao and E. Oset, Eur. Phys. J. A **49**, 139 (2013) [arXiv:1305.0786 [hep-ph]].
- [3] J. -J. Wu, R. Molina, E. Oset and B. S. Zou, Phys. Rev. Lett. **105**, 232001 (2010) [arXiv:1007.0573 [nucl-th]].
- [4] J. -J. Wu, R. Molina, E. Oset and B. S. Zou, Phys. Rev. C **84**, 015202 (2011) [arXiv:1011.2399 [nucl-th]].
- [5] M. Bando, T. Kugo, S. Uehara, K. Yamawaki and T. Yanagida, Phys. Rev. Lett. **54**, 1215 (1985).
- [6] M. Bando, T. Kugo and K. Yamawaki, Phys. Rept. **164**, 217 (1988).
- [7] U. G. Meissner, Phys. Rept. **161**, 213 (1988).
- [8] H. Nagahiro, L. Roca, A. Hosaka and E. Oset, Phys. Rev. D **79**, 014015 (2009) [arXiv:0809.0943 [hep-ph]].
- [9] M. F. M. Lutz and C. L. Korpa, Phys. Lett. B **633**, 43 (2006) [nucl-th/0510006].
- [10] L. Tolos, J. Schaffner-Bielich and H. Stoecker, Phys. Lett. B **635**, 85 (2006) [nucl-th/0509054].
- [11] T. Mizutani and A. Ramos, Phys. Rev. C **74**, 065201 (2006) [hep-ph/0607257].
- [12] L. Tolos, A. Ramos and T. Mizutani, Phys. Rev. C **77**, 015207 (2008) [arXiv:0710.2684 [nucl-th]].
- [13] J. -J. Wu and B. S. Zou, Phys. Lett. B **709**, 70 (2012) [arXiv:1011.5743 [hep-ph]].
- [14] N. Isgur and M. B. Wise, Phys. Lett. B **232**, 113 (1989).
- [15] M. Neubert, Phys. Rept. **245**, 259 (1994) [hep-ph/9306320].
- [16] A.V. Manohar and M.B. Wise. Heavy Quark Physics, Cambridge Monographs on Particle Physics, Nuclear Physics and Cosmology, vol. 10. Camb. Monogr. Part. Phys. Nucl. Phys. Cosmol.10,1
- [17] M. B. Wise, Phys. Rev. D **45**, 2188 (1992).
- [18] C. Garcia-Recio, V. K. Magas, T. Mizutani, J. Nieves, A. Ramos, L. L. Salcedo and L. Tolos, Phys. Rev. D **79**, 054004 (2009) [arXiv:0807.2969 [hep-ph]].
- [19] J. M. Flynn, E. Hernandez and J. Nieves, Phys. Rev. D **85**, 014012 (2012) [arXiv:1110.2962 [hep-ph]].
- [20] C. Garcia-Recio, J. Nieves, O. Romanets, L. L. Salcedo and L. Tolos, Phys. Rev. D **87**, 034032 (2013) [arXiv:1210.4755 [hep-ph]].
- [21] O. Romanets, L. Tolos, C. Garcia-Recio, J. Nieves, L. L. Salcedo and R. G. E. Timmermans, Phys. Rev. D **85**, 114032 (2012) [arXiv:1202.2239 [hep-ph]].
- [22] F. -K. Guo, C. Hidalgo-Duque, J. Nieves and M. P. Valderrama, Phys. Rev. D **88**, 054014 (2013) [arXiv:1305.4052 [hep-ph]].

- [23] C. Garcia-Recio, J. Nieves, O. Romanets, L. L. Salcedo and L. Tolos, *Phys. Rev. D* **87**, 074034 (2013) [arXiv:1302.6938 [hep-ph]].
- [24] O. Romanets, L. Tolos, C. Garca-Recio, J. Nieves, L. L. Salcedo and R. Timmermans, *Nucl. Phys. A* **914**, 488 (2013) [arXiv:1212.3943 [hep-ph]].
- [25] E. J. Garzon and E. Oset, *Eur. Phys. J. A* **48**, 5 (2012) [arXiv:1201.3756 [hep-ph]].
- [26] W. H. Liang, C. W. Xiao and E. Oset, *Phys. Rev. D* **89**, 054023 (2014) [arXiv:1401.1441 [hep-ph]].
- [27] W. H. Liang, T. Uchino, C. W. Xiao and E. Oset, *Eur. Phys. J. A* **51** (2015) 2, 16 [arXiv:1402.5293 [hep-ph]].
- [28] R. C. Carrasco and E. Oset, *Nucl. Phys. A* **536**, 445 (1992).
- [29] D. Gamermann, J. Nieves, E. Oset and E. Ruiz Arriola, *Phys. Rev. D* **81**, 014029 (2010) [arXiv:0911.4407 [hep-ph]].
- [30] D. Gamermann, http://ific.uv.es/nucth/tesis_DanGam.pdf
- [31] E. Oset, A. Ramos and C. Bennhold, *Phys. Lett. B* **527**, 99 (2002) [Erratum-ibid. B **530**, 260 (2002)] [nucl-th/0109006].
- [32] K. P. Khemchandani, A. Martinez Torres, H. Kaneko, H. Nagahiro and A. Hosaka, *Phys. Rev. D* **84**, 094018 (2011) [arXiv:1107.0574 [nucl-th]].
- [33] K. P. Khemchandani, H. Kaneko, H. Nagahiro and A. Hosaka, *Phys. Rev. D* **83**, 114041 (2011) [arXiv:1104.0307 [hep-ph]].
- [34] K. P. Khemchandani, A. Martinez Torres, H. Nagahiro and A. Hosaka, *Phys. Rev. D* **85**, 114020 (2012) [arXiv:1203.6711 [nucl-th]].
- [35] E. Oset, A. Ramos, E. J. Garzon, R. Molina, L. Tolos, C. W. Xiao, J. J. Wu and B. S. Zou, *Int. J. Mod. Phys. E* **21**, 1230011 (2012) [arXiv:1210.3738 [nucl-th]].
- [36] E. Oset and A. Ramos, *Nucl. Phys. A* **679**, 616 (2001) [nucl-th/0005046].
- [37] A. Pich, *Rept. Prog. Phys.* **58**, 563 (1995) [hep-ph/9502366].
- [38] B. Borasoy, *Phys. Rev. D* **59**, 054021 (1999) [hep-ph/9811411].
- [39] A. Bramon, A. Grau and G. Pancheri, *Phys. Lett. B* **344**, 240 (1995).
- [40] E. Oset, J. R. Pelaez and L. Roca, *Phys. Rev. D* **67**, 073013 (2003) [hep-ph/0210282].
- [41] D. Gamermann, E. Oset and B. S. Zou, *Eur. Phys. J. A* **41**, 85 (2009) [arXiv:0805.0499 [hep-ph]].
- [42] Talk of Juan Nieves at the Workshop on Hadron Physics, Troia (Turkey), 2009, <http://troia14.ozyegin.edu.tr/Home.html>
- [43] J. J. Wu, T.-S. H. Lee and B. S. Zou, *Phys. Rev. C* **85**, 044002 (2012) [arXiv:1202.1036 [nucl-th]].
- [44] S. G. Yuan, K. W. Wei, J. He, H. S. Xu and B. S. Zou, *Eur. Phys. J. A* **48**, 61 (2012) [arXiv:1201.0807 [nucl-th]].
- [45] J. Hofmann and M. F. M. Lutz, *Nucl. Phys. A* **763**, 90 (2005) [hep-ph/0507071].